Accepted version of the paper published in Structural Control and Health Monitoring, 25(12):e2270. 2018, https://doi.org/10.1002/stc.2270.
Corresponding author: altay@lbb.rwth-aachen.de

# A semi-active tuned liquid column damper for lateral vibration control of high-rise structures: Theory and experimental verification

Okyay Altay, Sven Klinkel

*Department of Civil Engineering, RWTH Aachen University*
*Mies-van-der-Rohe-Str. 1, 52074 Aachen, Germany*

**Abstract**

This paper presents a new type of semi-active tuned liquid column damper (S-TLCD) for the lateral vibration control of high-rise civil engineering structures. Analogous to the passive tuned liquid column damper (TLCD), the S-TLCD comprises a U-shaped tank consisting of two vertical columns, which are arranged at a distance from each other and communicating through a horizontal passage. The tank is partially filled with a Newtonian fluid until the liquid reaches a certain level in the columns. In contrast to the passive TLCD, the S-TLCD provides also mechanisms for a continuous adaptation of both its natural frequency and damping behaviour in real-time. In the first part of the paper, the governing equations of the S-TLCD are derived based on the Bernoulli equation of a non-stationary incompressible liquid flow. The natural frequency of the S-TLCD is revealed to depend on the scaled length of the liquid. The scaling amount of the liquid length is formulated in dependence of the cross-sectional area ratios of the tank segments. The mathematical description of the S-TLCD is concluded by providing the state-space representation of a multi-degree-of-freedom structure with several S-TLCDs. In the second part of the paper, the derived natural frequency equation is verified and the proof of concept of the S-TLCD is shown by experimental investigations, which are performed on an S-TLCD model utilizing a test structure and shaking table tests.

*Keywords:* Semi-active tuned liquid column dampers; adaptive stiffness; adaptive damping; natural frequency tuning; high-rise structures; lateral vibrations

## 1. Introduction

Semi-active damper systems can adapt themselves to the changing structural conditions and loading situations based on the data captured by their sensors. This autonomous tuning capability allows the semi-active structural control devices to outperform passive vibration mitigation methods. Furthermore, semi-active systems can alternate their parameters also in real-time ensuring a superior, stable and low-energy control performance compared to active systems. In the last decades, many semi-active systems have been developed. However, most of these devices can adapt only their damping parameters. Besides the active variable stiffness (AVS) system developed by Kobori et al. [1], only a few semi-active systems have been developed with stiffness adaptation capabilities. Some rare examples include the adaptive length pendulum tuned mass dampers (APTMD) developed by Nagarajaiah, which are also applied in the USA, Japan and China [2–4]. Semi-active systems with tunable natural frequency capabilities are especially necessary for slender high-rise structures, such as wind turbines. During the service time, these structures change their natural frequencies due to degradation and soil effects. Thereby passive systems lose their

efficiency by frequency off-tuning. In this context, Sun developed for wind turbines subjected to multi-hazards a sophisticated simulation environment, where degradation and soil effects can be simulated [5, 6]. He proposed and investigated for monopile offshore wind turbines a semi-active tuned mass damper (STMD), which can adapt its damping and frequency parameters. The results show a significant improvement of the control system due to semi-active adaptation capability.

Besides these mechanical tuned mass dampers, the so far proposed liquid based tuned mass dampers, which possess both natural frequency and damping adaptation capabilities, are still in the very early development stage. Due to their geometric versatility, low prime costs and stable dynamic behaviour, the tuned liquid column dampers (TLCD) are regarded as one of the most promising solutions. However, an applicable semi-active TLCD with continuously variable natural frequency does not exist yet.

First invented by Frahm [7] already in 1909 for ships and then proposed by Sakai [8] in 1991 for civil engineering structures, the TLCD is one of the first structural control devices. The TLCD consists of a U-shaped tube with two vertical columns, which are open at one end and connected at the other end by a horizontal segment. The tube is attached on a structure, the vibrations of which are to be controlled. For high-rise structures the TLCDs are usually attached at the top of the structure, where the maximum lateral motion is expected. The tube is partially filled with a Newtonian fluid, which is prescribed to flow with phase shift with respect to the structure. The phase shift must be tuned by the natural frequency and the damping parameters of the liquid motion. The oscillating liquid mass evokes restoring forces. During this oscillation local friction and turbulence effects in the tube dissipate vibration energy, allowing a control of the structural vibrations.

To tune the damping of the TLCDs, Sakai installed an orifice in the horizontal segment. This orifice can be closed manually to introduce additional damping by increasing the local friction [8]. Frahm and Matsuo closed the open ends of the vertical columns with orifices, which influence the air flow and reduce the speed of liquid level motion [7, 9]. As this method influences also the natural frequency, the approach proposed by Sakai counts as an established method for the damping tuning of the TLCDs. Several studies have been conducted considering the calculation and control of the damping effects introduced by the orifice, such as by Yalla and La et al. In their study, Yalla et al. equipped a TLCD with an electro-pneumatic valve to tune its inherent damping in a semi-active manner [10]. They developed a control strategy and conducted experimental investigations. The results show that the semi-active tuning of the inherent damping provides the TLCD an up-to 25% performance improvement. Furthermore, La et al. derived in their study a general on-off controller for the damping tuning of the TLCDs using the orifice [11]. They documented the robust performance of the controller numerically using a five-degree-of-freedom shear frame, which is subjected to earthquake. Both of these investigations use TLCDs without frequency adaptation capabilities.

On the other hand, to tune the natural frequency of the TLCDs, Csupor divided the horizontal segment into two channels, each with a different cross-sectional area [12]. As the fluid flow velocity in the tube depends on the cross-sectional area, this approach allowed the TLCD to switch between two natural frequencies. However, for the mitigation of lateral vibrations the volume of the horizontal segment is decisive. Therefore, the TLCD proposed by Csupor alternates unfavorably also its restoring force level depending on the volume of the chosen channel.

Another approach for the natural frequency tuning was proposed by Nomichi et al. [13]. By sealing the open ends of the vertical columns they introduced an air spring, which increased the natural frequency of the liquid oscillation. Yoshimura et al. enhanced this approach by sensors and a controller to tune the natural frequency in a semi-active manner [14]. Kagawa et al. divided the vertical column above the liquid level into several chambers, which are connected by orifices [15, 16]. By closing the orifices, the air volume is modulated causing also an adjustment of the stiffness coefficient of the air spring. This allowed the TLCD to switch its natural frequency incrementally. Hochrainer et al. investigated the application of this sealed tuned liquid column gas damper (TLCGD) on structures [17–19]. Reiterer et al. implemented TLCGD in vertical direction [20]. The first application of TLCGD showed that the approach using overpressure is eligible primarily for small-scale distributed TLCD systems [21]. Moreover, as the supplementary air spring increases the natural frequency of the TLCD, it impedes the application of the damper on slender structures, which usually oscillate with low frequencies.

A further method for frequency tuning is proposed by Yoshimura et al. [22]. They integrated in TLCDs

mechanical spring elements influencing the flow velocity of the liquid. They attached the liquid column damper with period adjustment (LCD-PA) on a hotel building in Tokyo [23]. Also Ghosh and Sonmez et al. changed the natural frequency of the TLCD by interposing spring elements between TLCD and structure [24–26]. Both of these hybrid solutions control the natural frequency mechanically using spring elements while the TLCD continues its operation in a passive manner.

Kim et al. divided the vertical columns in upright cells allowing a frequency tuning of the TLCD [27]. They applied this TLCD on four skyscrapers in South Korea to tune the natural frequency after installation of the damper in a passive adaptive manner. By closing the chambers, the cross-sectional area of the columns can be adjusted, which influences the liquid flow speed and enables an incremental frequency tuning.

This paper introduces a new type semi-active tuned liquid column damper (S-TLCD), which can change both its natural frequency and damping continuously. Section 2 presents the general properties of the S-TLCD. Section 3 derives the governing equations of the S-TLCD including its equation of motion, natural frequency and state-space representation. Section 4 verifies the natural frequency equation and shows the proof of concept of the S-TLCD experimentally by using a small-scale model of the S-TLCD and performing shaking table tests. Section 5 concludes the mathematical definition and the results of the experimental studies.

## 2. Semi-active Tuned Liquid Column Damper

Inspired by the passive TLCD, the S-TLCD is a tank filled with a Newtonian liquid, such as a mixture of water and antifreeze. The tank has a U-shaped geometry consisting of two rectangular liquid columns, which are arranged at a distance from each other and communicating by a horizontal passage as shown in Figure 1. In the tank, mechanisms for tuning both the natural frequency and the damping are provided, which can adjust the parameters of the damper in real-time. For this purpose, perpendicular to the flow direction, movable vertical panels are attached to the column walls, which allow to change the cross-sectional area of the columns without changing the horizontal distance between the liquid columns. By changing the cross-sectional area, the velocity of the liquid flow can be controlled enabling the natural frequency tuning capability of the S-TLCD. Each movable panel consists of a transition and an upright segment. The liquid level oscillates in the upright segment range allowing the S-TLCD to keep its natural frequency constant during its operation. The gaps between movable panels and column walls are sealed by waterproof elastic membranes. For the tuning of the damping, several butterfly valves are installed in the connection passage of the liquid columns. By closing these valves, local friction effects can be introduced allowing an increase in damping. The motion of the panels and the butterfly valves is controlled by actuators. The liquid motion is measured by a capacitance transducer. A demonstrator of S-TLCD with such actuators and sensors will be presented in Section 4.1.

## 3. Mathematical Description

In fluid dynamics, the absolute acceleration $\mathbf{a}$ of a single liquid particle with infinitesimal mass $\mathrm{d}m$ and volume $\mathrm{d}V$ is determined by the surrounding force field $\mathbf{f}$, such as gravity, and the pressure gradient $\operatorname{grad} p$, as defined by the Euler impulse equation for homogeneous frictionless incompressible fluids in Eq. 1, [28]. In Eq. 2 the terms are divided by the liquid density $\rho$. Besides gravity, magnetism and electricity cause also a force field, which can be used to control magnetorheological or electrorheological liquids.

$$\mathrm{d}m\,\mathbf{a} = \mathrm{d}m\,\mathbf{f} - \mathrm{d}V \operatorname{grad} p \tag{1}$$

$$\Leftrightarrow \mathbf{a} = \mathbf{f} - \frac{1}{\rho} \operatorname{grad} p \tag{2}$$

Figure 2 shows the liquid particle moving through a tube between the ① and ② with the cross-sectional areas $A_1$ and $A_2$ accordingly. The starting and ending velocities of the particle are $\mathbf{v_1}$ and $\mathbf{v_2}$. The direction

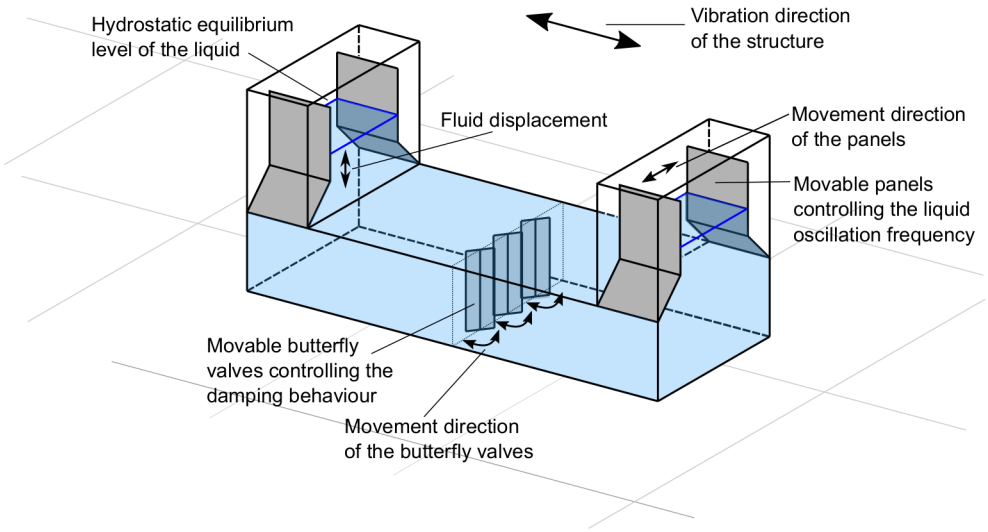


Figure 1: The proposed semi-active tuned liquid column damper (S-TLCD) with natural frequency and damping tuning capabilities.

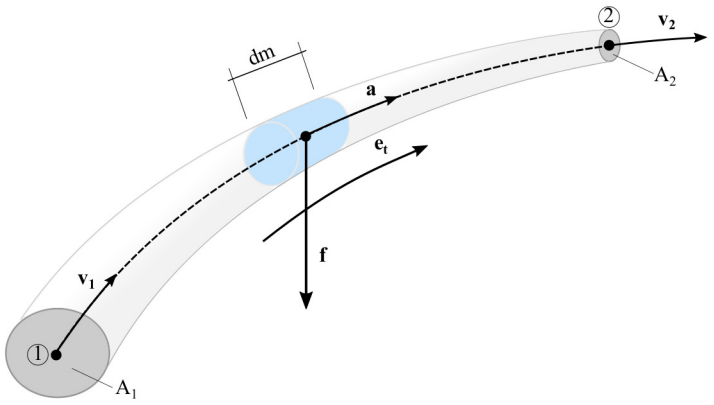


Figure 2: Homogeneous frictionless incompressible fluid particle moving through a tube from ① to ②.

vector tangent to the tube streamline is labeled as $\mathbf{e_t}$. The force field $\mathbf{f}$ acting on the particle and the absolute acceleration $\mathbf{a}$ of the liquid particle are also shown in Figure 2.

Based on Eq. 2 Sakai et al. [29] derived the equation of motion of passive TLCDs attached to horizontally vibrating high-rise structures. Xue et al. [30] enhanced this equation for pitching structures. Hochrainer et al. [17] derived the equation of motion for TLCGDs attached to horizontally vibrating high-rise structures according to the approach developed by Sakai. Reiterer et al. [31] enhanced this equation for TLCGDs attached to vertically and rotationally oscillating structures, such as footbridges. In this section, the governing equations of the S-TLCD, which is attached to a horizontally vibrating high-rise structure, will be derived in a similar manner based on the Bernoulli equation of the non-stationary incompressible flow of the liquid.

### *3.1. Equation of Motion*

The total acceleration of a liquid column in a tank can be calculated in a general form by integrating the Eq. 2 along the streamline for the force field of gravity $\mathbf{g}$ leading to

$$\int \mathbf{a} \cdot \mathbf{e_t} \mathrm{d}s = \int \mathbf{g} \cdot \mathbf{e_t} \mathrm{d}s - \frac{1}{\rho} \int \mathrm{grad}\, p \cdot \mathbf{e_t} \mathrm{d}s. \tag{3}$$

The integral of the pressure gradient along the streamline of the S-TLCD equals to the pressure loss $\Delta p$, which is caused by turbulance and local friction effects in the tank. Analytical methods for the calculation of pressure loss can be found in the literature, such as in Eq. 4 according to [30]

$$\Delta p = \delta \rho |\dot{u}| \dot{u}, \tag{4}$$

where $\dot{u}$ is the velocity of the liquid flow and $\delta$ the head loss coefficient, which is a function representing the turbulence effects depending on Reynolds number of the liquid stream together with the local friction effects. The absolute liquid acceleration $\mathbf{a}$ in Eq. 3 is defined as the sum of the acceleration $\mathbf{a_M}$ of the main structure, on which the S-TLCD is attached, and the relative acceleration $\mathbf{a'}$ of the liquid column yielding

$$\mathbf{a} \cdot \mathbf{e_t} = \mathbf{a_M} \cdot \mathbf{e_t} + \mathbf{a'} \cdot \mathbf{e_t}. \tag{5}$$

The relative acceleration $\mathbf{a'}$ of the fluid is separated into local and convective accelerations as shown below in Eq. 6. The local acceleration describes the force field induced time-dependent change in the velocity $\dot{u}$ of the liquid particle. The convective acceleration describes the position-dependent change in the velocity of the liquid stream.

$$\mathbf{a'} \cdot \mathbf{e_t} = \frac{\partial \dot{u}}{\partial t} + \dot{u} \frac{\partial \dot{u}}{\partial s} \tag{6}$$

From Eq. 3, by integrating the scalar product $\mathbf{g} \cdot \mathbf{e_t}$ and using the pressure loss $\Delta p$ as described before in Eq. 4, a modified version of the Bernoulli equation can be determined for the S-TLCD as shown in Eq. 7, where $u$ is the displacement of the liquid in the tank.

$$\int \mathbf{a_M} \cdot \mathbf{e_t} \mathrm{d}s + \int \frac{\partial \dot{u}}{\partial t} \mathrm{d}s + \int \frac{\partial}{\partial s} \left( \frac{\dot{u}^2}{2} \right) \mathrm{d}s = -2gu - \frac{1}{\rho} \Delta p \tag{7}$$

As shown in Figure 3, the main parameters describing the geometry of the S-TLCD tank are in vertical direction the height $V$ and in horizontal direction the length $H$ of the streamline. Further parameter is $d_i$, where $i = [1, 4]$ giving the cross-sectional areas of the vertical columns and the horizontal passage. As seen in the side view, the cross-sectional area of the vertical columns can change depending on the inclination angle $\beta$ of the movable panels. The vertical columns are hereby divided into three sections: beginning section, transition section and end section, $V_1$, $V_2$ and $V_3$ respectively. The height $V_2$ is a function of $\beta$ and furthermore, for S-TLCDs with constant liquid amount also $V_3$ changes depending on $\beta$.

The cross-sectional areas of the tank are calculated using Eq. 8 and 10. Hereby, $A_{V1}$ is the cross-sectional area of the column-top, $A_{V2}$ is the cross-sectional area of the column-beginning and $A_H$ is the cross-sectional

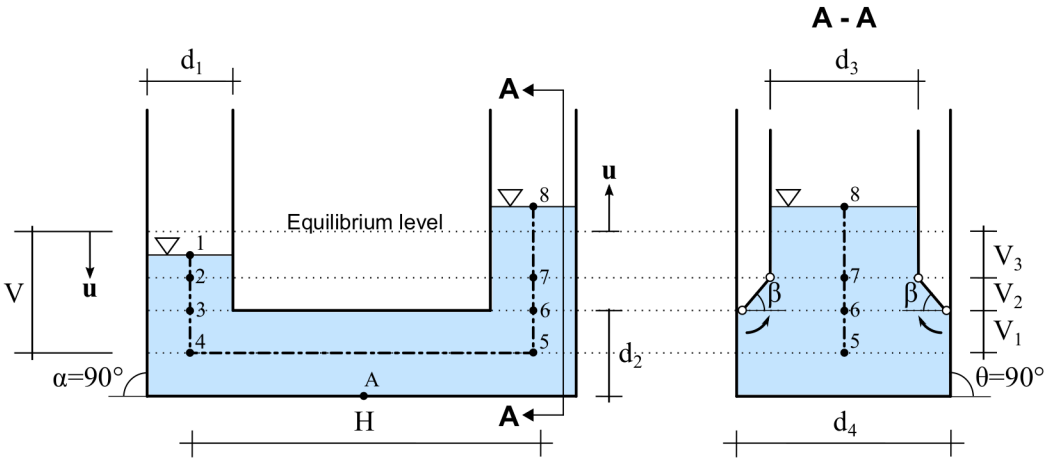


Figure 3: Mechanical model showing the governing parameters of the S-TLCD. Left: Front view of the S-TLCD. Right: Side view of the S-TLCD.

area of the connecting passage of the vertical columns. Because $d_3$ is a function of the panel position $\beta$, $A_{V1}$ can be modified by changing $\beta$.

$$A_{V1} = d_1 d_3 \tag{8}$$
$$A_{V2} = d_1 d_4 \tag{9}$$
$$A_H = d_2 d_4 \tag{10}$$

The calculation of the acceleration effects, which are induced by the oscillations of the main structure, are performed in Eq. 11, along the streamline through connection points 1-8 of the sections of the damper tank as shown in Figure 3. Here, the acceleration of the main structure is assumed to occur only in horizontal $x$-direction, which is usually the relevant vibration direction for high-rise structures subjected to wind and earthquake loads. Therefore, for the acceleration, it is assumed that $\mathbf{a_M} = \ddot{x}\,\mathbf{e_x}$. The scalar product of the horizontal direction vector $\mathbf{e_x}$ with $\mathbf{e_t}$ vector, which is parallel to the streamline, is conducted in Eq. 12-14. The result equals to the length of the horizontal passage of the damper $H$ multiplied with the acceleration $\ddot{x}$ of the main structure.

$$\int \mathbf{a_M} \cdot \mathbf{e_t} \mathrm{d}s = \ddot{x} \left( \int_1^2 \mathbf{e_x} \cdot \mathbf{e_t} \mathrm{d}s + \int_2^3 \mathbf{e_x} \cdot \mathbf{e_t} \mathrm{d}s + \cdots + \int_7^8 \mathbf{e_x} \cdot \mathbf{e_t} \mathrm{d}s \right) = H\ddot{x} \tag{11}$$

$$1 \longrightarrow 4: \quad \mathbf{e_x} \cdot \mathbf{e_t} = 0 \tag{12}$$
$$4 \longrightarrow 5: \quad \mathbf{e_x} \cdot \mathbf{e_t} = 1 \tag{13}$$
$$5 \longrightarrow 8: \quad \mathbf{e_x} \cdot \mathbf{e_t} = 0 \tag{14}$$

Figure 4 shows the velocity profile of the liquid stream in the S-TLCD. The velocity changes in dependence with the cross-sectional area of each segment. This is applied in Eq. 15-23 to determine the local acceleration of the liquid flow. The result corresponds to the acceleration $\ddot{u}$ of the liquid scaled by $L_1$, which we call first effective length of the S-TLCD. Eq. 16 determines $L_1$ by solving the integral in Eq. 15. For a TLCD with equal horizontal and vertical cross-sections $A_H = A_V$, the effective length corresponds to the total length of the liquid streamline.

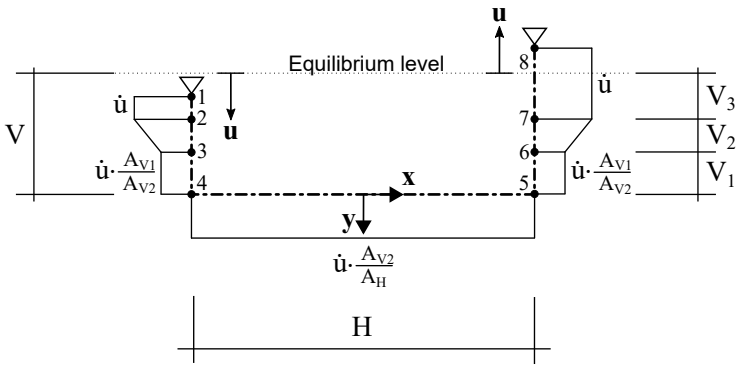


Figure 4: Velocity profile of the liquid stream in the damper tank.

$$\int \frac{\partial \dot{u}}{\partial t} \mathrm{d}s = \sum_{i=1}^{7} \int_{i}^{i+1} \frac{\partial \dot{u}}{\partial t} \mathrm{d}s = L_1 \ddot{u} \tag{15}$$

$$L_1 = 2V_3 + V_2 + (2V_1 + V_2)\frac{A_{V1}}{A_{V2}} + H\frac{A_{V1}}{A_H} \tag{16}$$

$$1 \longrightarrow 2: \quad \frac{\partial \dot{u}}{\partial t} = \ddot{u} \tag{17}$$

$$2 \longrightarrow 3: \quad \frac{\partial \dot{u}}{\partial t} = \frac{\ddot{u}}{2}\left(1 + \frac{A_{V1}}{A_{V2}}\right) \tag{18}$$

$$3 \longrightarrow 4: \quad \frac{\partial \dot{u}}{\partial t} = \ddot{u}\frac{A_{V1}}{A_{V2}} \tag{19}$$

$$4 \longrightarrow 5: \quad \frac{\partial \dot{u}}{\partial t} = \ddot{u}\frac{A_{V1}}{A_H} \tag{20}$$

$$5 \longrightarrow 6: \quad \frac{\partial \dot{u}}{\partial t} = \ddot{u}\frac{A_{V1}}{A_{V2}} \tag{21}$$

$$6 \longrightarrow 7: \quad \frac{\partial \dot{u}}{\partial t} = \frac{\ddot{u}}{2}\left(1 + \frac{A_{V1}}{A_{V2}}\right) \tag{22}$$

$$7 \longrightarrow 8: \quad \frac{\partial \dot{u}}{\partial t} = \ddot{u} \tag{23}$$

As shown in Eq. 24, due to the symmetry of the damper the integral of the convective acceleration becomes zero:

$$\int_1^8 \frac{\partial}{\partial s}\left(\frac{\dot{u}^2}{2}\right) \mathrm{d}s = \frac{1}{2}(\dot{u}_8^2 - \dot{u}_1^2) = 0. \tag{24}$$

The sum of Eq. 11, 15 and 24 gives according to Eq. 7 the expanded nonlinear equation of motion of the S-TLCD for a liquid motion along the streamline as shown in Eq. 25 and modified in Eq. 26, where $\omega_D$ is the adaptable natural circular frequency of the semi-active damper, which is calculated according to Eq. 27. In Eq. 26, we call the parameter $\gamma_1$ as the first geometric factor of the S-TLCD, which is given by Eq. 28. Both $\omega_D$ and $\gamma_1$ depend on the first effective length of the streamline $L_1$. By changing the cross-sectional area of the vertical liquid columns, the effective length and following that the circular frequency $\omega_D$ and the geometric factor $\gamma_1$ change.

As a result, the equation of motion of the S-TLCD reads

$$L_1\ddot{u} + 2gu + \frac{1}{\rho}\Delta p = -H\ddot{x}, \tag{25}$$

$$\Leftrightarrow \ddot{u} + \omega_D^2 u + \delta|\dot{u}|\dot{u} = -\gamma_1\ddot{x}, \tag{26}$$

where the natural frequency of the S-TLCD is given by

$$\omega_D = \sqrt{\frac{2\,g}{L_1}} \tag{27}$$

and the first geometric factor of the S-TLCD is expressed as

$$\gamma_1 = \frac{H}{L_1}. \tag{28}$$

As shown in Eq. 27, the natural frequency $\omega_D$ of the S-TLCD depends only on the first effective length $L_1$ . This equation and the calculation of the first effective length $L_1$ accordingly will be verified experimentally in Section 4.2.

In the equation of motion of the S-TLCD, the nonlinear term $\delta|\dot{u}|\dot{u}$ can be linearized according to [31] into $2D_D\omega_D\dot{u}$, where $D_D$ is the equivalent viscous damping ratio of the S-TLCD. The $D_D$ can be calculated by demanding for both linear and nonlinear cases that the energy dissipation is for each cycle equal. This yields the relation shown in Eq. 29, where $T$ is the vibration period.

$$\int_0^T |\left(\delta|\dot{u}|\dot{u} + \omega_D^2 u\right)\dot{u}|\mathrm{d}t = \int_0^T |\left(2D_D\omega_D\dot{u} + \omega_D^2 u\right)\dot{u}|\mathrm{d}t \tag{29}$$

As described in [31], from Eq. 29 by substituting the time harmonic function $u = U_0\cos\omega_D t$, the equivalent viscous damping ratio $D_D$ is determined proportional to the vibration amplitude $U_0$ as shown in Eq. 30.

$$D_D = \frac{4U_0\delta}{3\pi} \tag{30}$$

Using this approach the equation of motion of the S-TLCD can be linearized as

$$\ddot{u} + \omega_D^2 u + 2D_D\omega_D\dot{u} = -\gamma_1\ddot{x}. \tag{31}$$

This approach simplifies, at least for the harmonic excitations, the tuning of the damping. However, especially in case of random excitations with changing amplitudes, for an accurate tuning of the damping, the nonlinear term $\delta|\dot{u}|\dot{u}$ given in Eq. 26 should be used. The accurate tuning of this parameter can be accomplished by using soft-computing methods such as Fuzzy control, neural networks and evolutionary algorithms [32], which is the subject of future research.

### *3.2. Restoring Force*

The restoring force of the S-TLCD on a horizontally oscillating high-rise structure is derived from the momentum equation. The momentum $\mathbf{I}$ induced by the liquid motion is computed in Eq. 32 using the integral of the resulting liquid velocity over the liquid mass $m_f$. The resulting velocity is assembled by the velocity of the structure $\mathbf{v_A}$ at the attachment point $A$ of the S-TLCD to the structure and the liquid velocity $\mathbf{v}$.

$$\mathbf{I} = \int(\mathbf{v_A} + \mathbf{v})\mathrm{d}m_f = \int_1^8 \left(\dot{x}\mathbf{e_t} + \dot{u}\frac{A_{V1}}{A(s)}\mathbf{e_t}\right)\rho A(s)\mathrm{d}s \tag{32}$$

The momentum projected in lateral $x$-direction is computed in Eq. 33. The restoring force is determined in Eq. 34 from the time derivative of the momentum equation. In Eq. 35, the liquid mass $m_f$ is calculated. The second geometric factor $\gamma_2$ is calculated in Eq. 36 and the second efficient length $L_2$ is given in Eq. 37.

$$I_x = \rho \left[ A_{V1} 2V_3 \dot{x} + (A_{V1} + A_{V2}) V_2 \dot{x} + A_{V2} 2V_1 \dot{x} + A_H H \left( \dot{x} + \dot{u} \frac{A_{V1}}{A_H} \right) \right] \tag{33}$$

$$F_x = \frac{\mathrm{d}I_x}{\mathrm{d}t} = m_f (\ddot{x} + \gamma_2 \ddot{u}) \tag{34}$$

$$m_f = \rho A_{V1} L_2 \tag{35}$$

$$\gamma_2 = \frac{H}{L_2} \tag{36}$$

$$L_2 = 2V_3 + V_2 + (2V_1 + V_2) \frac{A_{V2}}{A_{V1}} + H \frac{A_H}{A_{V1}} \tag{37}$$

The equation of motion of a single-degree-of-freedom (SDoF) system with an S-TLCD subjected to a time-dependent load $F(t) = f(t) m_S$ is shown in Eq. 38, where $\mu = m_f / m_S$ is the ratio of the liquid mass to the modal mass of the structure. In the same equation, the damper interaction forces are represented by $\mu\ddot{x} + \mu\gamma_2\ddot{u}$, which is derived previously in Eq. 34. In Eq. 38, $\omega_S$ is the natural frequency of the structure and $D_S$ is the damping ratio.

$$\ddot{x} + 2 D_S \omega_S \dot{x} + \omega_S^2 x = -\mu\ddot{x} - \mu\gamma_2\ddot{u} + f \tag{38}$$

If the structure is subjected to a ground acceleration $\ddot{x}_g$, the equation of motion of the SDoF system with the S-TLCD is rewritten as

$$\ddot{x} + 2\, D_S \omega_S \dot{x} + \omega_S^2 x = -\ddot{x}_g - \mu\, (\ddot{x} + \ddot{x}_g) - \mu\gamma_2\ddot{u} + f. \tag{39}$$

Based on this equation, the equation of motion of a multi-degree-of-freedom (MDoF) system with several S-TLCDs will be derived in Section 3.4 by using the state-space representation.

### *3.3. Geometric Factors*

The geometric factors $\gamma_1$ and $\gamma_2$ determine the ratio of the horizontal length $H$ of the S-TLCD to the efficient lengths $L_1$ and $L_2$. For an S-TLCD with a constant liquid amount, the cross-sectional area $A_{V1}$, the height $V_2$ and the height $V_3$ depend on $\beta$. As a result, $L_1$ and $L_2$, as well as $\gamma_1$ and $\gamma_2$ accordingly, become also a function of $\beta$. For the sake of convenience, the equations of the efficient lengths and geometric factors representing this general case are enlisted below:

$$L_1(\beta) = 2V_3(\beta) + V_2(\beta) + (2V_1 + V_2(\beta)) \frac{A_{V1}(\beta)}{A_{V2}} + H \frac{A_{V1}(\beta)}{A_H}, \tag{40}$$

$$L_2(\beta) = 2V_3(\beta) + V_2(\beta) + (2V_1 + V_2(\beta)) \frac{A_{V2}}{A_{V1}(\beta)} + H \frac{A_H}{A_{V1}(\beta)}, \tag{41}$$

$$\gamma_1(\beta) = \frac{H}{L_1(\beta)}, \tag{42}$$

$$\gamma_2(\beta) = \frac{H}{L_2(\beta)}. \tag{43}$$

For a TLCD with uniform cross-sectional area, the total length of the liquid column $L$ equals to both $L_1$ and $L_2$. For a TLCD with a constant cross-sectional area of the vertical columns $A_V$ and a different cross-sectional area of the horizontal passage $A_H$, as proposed by Hitchcock et al. [33, 34], both efficient lengths $L_1$ and $L_2$ are given by the sum of the total liquid length in vertical direction and the horizontal length, which is scaled by the ratio of the cross-sectional areas $A_V$ and $A_H$. For this type of TLCD, if the

liquid amount is constant, a change of $A_V$ would influence the first efficient length $L_1$ linearly and the second efficient length $L_2$ in a nonlinear manner. In case of the S-TLCD with a constant liquid amount, a change of the panel position $\beta$ influences both $L_1$ and $L_2$ nonlinearly. As the natural frequency $\omega_D$ depends also on $L_1$, a change of the panel position $\beta$ will also cause $\omega_D$ and consequently the geometric factors $\gamma_1$ and $\gamma_2$ to change in a nonlinear manner. This effect can be seen in Sections 4.2 and 4.3 from the experimental results.

The interaction forces between S-TLCD and structure are scaled by $\gamma_1$ and $\gamma_2$. Therefore, the geometric factors are expected to effect the efficiency of the damper depending on $\beta$. The first geometric factor $\gamma_1$ scales the acceleration of the structure $\ddot{x}$, as given in the equation of motion of the S-TLCD in Eq. 31. Accordingly, together with the acceleration $\ddot{x}$ of the structure, an increase in the geometric factor $\gamma_1$ amplifies the liquid motion amplitude $u$.

In the equation of motion of the structure, given in Eq. 39, the second geometric factor $\gamma_2$ scales the acceleration of the liquid motion with the term $-\mu\,\gamma_2\,\ddot{u}$, where the minus sign represents the restoring character of the interaction force. Consequently, an increase in the geometric factor $\gamma_2$ mitigates the lateral motion $x$ of the structure.

From the arguments above, it can be assumed that $\gamma_2$ will dominate the efficiency of the S-TLCD. However, $\gamma_1$ correlates directly with $L_1$ and with the natural frequency $\omega_D$ accordingly, which is vital for the efficiency of the damper. This effect can also be observed from the experimental results presented in Section 4.2. Furthermore, to increase the active mass fraction of the S-TLCD, both $\gamma_1$ and $\gamma_2$ must be maximized, which will be shown below.

Analogous to the TLCD, the active mass fraction for the S-TLCD defines the amount of liquid mass participating to the structural control by inducing the restoring force. The rest of the liquid mass is necessary for the tuning of the natural frequency of the damper. The amount of active mass fraction can be determined according to Hochrainer et al. [17] by introducing the scaled liquid motion $\bar{u} = u/\gamma_1$ in the equations of motion of the structure and the S-TLCD, and by multiplying these equations with $\mathrm{diag}\,(1/(1+\mu\,(1-\gamma_1\,\gamma_2)), 1/\gamma_1)$, which yields

$$\begin{bmatrix} 1+\bar{\mu} & \bar{\mu} \\ 1 & 1 \end{bmatrix} \begin{bmatrix} \ddot{x} \\ \ddot{\bar{u}} \end{bmatrix} + \begin{bmatrix} 2\,\bar{D}_S\bar{\omega}_S & 0 \\ 0 & 2\,D_D\omega_D \end{bmatrix} \begin{bmatrix} \dot{x} \\ \dot{\bar{u}} \end{bmatrix} + \begin{bmatrix} \bar{\omega}_S^2 & 0 \\ 0 & \omega_D^2 \end{bmatrix} \begin{bmatrix} x \\ \bar{u} \end{bmatrix} = - \begin{bmatrix} 1+\bar{\mu} \\ 1 \end{bmatrix} \ddot{x}_g + \begin{bmatrix} 1/\bar{m}_S \\ 0 \end{bmatrix} f, \tag{44}$$

where the ratio between the active mass fraction $\bar{m}_D$ of the S-TLCD and the sum of the modal mass of the structure $m_S$ and the rest liquid mass of the damper is denoted by $\bar{\mu}$, which is given by

$$\bar{\mu} = \frac{\bar{m}_D}{\bar{m}_S} = \frac{m_D\gamma_1\gamma_2}{m_S\,(1+\mu\,(1-\gamma_1\gamma_2))} = \frac{\mu\gamma_1\gamma_2}{1+\mu\,(1-\gamma_1\gamma_2)}. \tag{45}$$

From the numerator of Eq. 45 it can be clearly seen, that the active mass fraction $\bar{m}_D$ equals to the total liquid mass of the damper scaled by $\gamma_1$ and $\gamma_2$:

$$\bar{m}_D = m_D\gamma_1\gamma_2. \tag{46}$$

In Eq. 44, $\bar{\omega}_S$ and $\bar{D}_S$ are given by dividing the natural frequency $\omega_S$ and the damping ratio $D_S$ by $\sqrt{1+\mu\,(1-\gamma_1\gamma_2)}$.

### *3.4. State-Space Representation*

In this section, the state-space representation of a $n$-DoF structure subjected to a horizontal ground acceleration $\ddot{x}_g$ and horizontal excitation forces $\mathbf{F}(\mathbf{t})$ with $k\times$ S-TLCDs will be derived. The equation of motion of the system is given in Eq. 47. In this equation, $\mathbf{M_M}$ is a hypermatrix consisting of the mass of the structure and the S-TLCDs. The lateral displacement vector of the system and the liquid motion vector of the S-TLCDs are denoted by $\mathbf{x}$ and $\mathbf{u}$ respectively. $\mathbf{C_S}$ and $\mathbf{C_D}$ are the damping matrices of the structure and the S-TLCDs. $\mathbf{K_S}$ and $\mathbf{K_D}$ are the stiffness matrices. $\mathbf{M_S}$ is the modal mass matrix of the structure and $\mathbf{M_D}$ is the mass matrix of the S-TLCDs. The vector $\mathbf{r}$ distributes the ground excitation $\ddot{x}_g$ to the DoFs

of the structure. As shown in Eq. 48, $\mathbf{r}$ is an identity vector for a horizontally excited structure with DoFs only in horizontal direction.

$$\mathbf{M_M} \cdot \begin{bmatrix} \ddot{\mathbf{x}} \\ \ddot{\mathbf{u}} \end{bmatrix} + \begin{bmatrix} \mathbf{C_S} & \mathbf{0} \\ \mathbf{0} & \mathbf{C_D} \end{bmatrix} \cdot \begin{bmatrix} \dot{\mathbf{x}} \\ \dot{\mathbf{u}} \end{bmatrix} + \begin{bmatrix} \mathbf{K_S} & \mathbf{0} \\ \mathbf{0} & \mathbf{K_D} \end{bmatrix} \cdot \begin{bmatrix} \mathbf{x} \\ \mathbf{u} \end{bmatrix} = - \begin{bmatrix} \mathbf{M_S} \cdot \mathbf{r} + \mathbf{L} \cdot \mathbf{M_D} \cdot \mathbf{i} \\ \mathbf{\Gamma_1} \cdot \mathbf{i} \end{bmatrix} \ddot{x}_g + \begin{bmatrix} \mathbf{f} \\ \mathbf{0} \end{bmatrix} \tag{47}$$

$$\mathbf{r}^{\mathrm{T}} = (1, 1, ..., 1)_{1 \times n} \tag{48}$$

The S-TLCDs are distributed to the DoFs of the structure by using an incidence matrix $\mathbf{L}$ with the dimension $n \times k$. Eq. 49 below shows an example of an incidence matrix for a structure with three DoF with two S-TLCDs attached to the second and third DoF of the structure.

$$\mathbf{L} = \begin{bmatrix} 0 & 0 \\ 1 & 0 \\ 0 & 1 \end{bmatrix} \tag{49}$$

For a horizontally excited system with all S-TLCDs also in the horizontal direction, the vector $\mathbf{i}$ is an identity vector as shown in Eq. 50.

$$\mathbf{i}^{\mathrm{T}} = (1, 1, ..., 1)_{1 \times k} \tag{50}$$

Furthermore, in Eq. 47, $\mathbf{\Gamma}_1$ is a matrix containing the geometric factors of the S-TLCDs. The excitation forces acting on the structure are represented by $\mathbf{f}$.

The hypermatrix $\mathbf{M_M}$ is assembled in Eq. 51. It contains besides the mass matrices $\mathbf{M_S}$ and $\mathbf{M_D}$, and the incidence matrix $\mathbf{L}$ also the matrices $\mathbf{\Gamma_1}$ and $\mathbf{\Gamma_2}$ with the geometric factors, as given in Eq. 52. The hypermatrix includes furthermore an identity matrix $\mathbf{I}$, as shown in Eq. 53.

$$\mathbf{M_M} = \begin{bmatrix} \mathbf{M_S} + \mathbf{L} \cdot \mathbf{M_D} \cdot \mathbf{L}^{\mathrm{T}} & \mathbf{L} \cdot \mathbf{M_D} \cdot \mathbf{\Gamma_2} \\ \mathbf{\Gamma_1} \cdot \mathbf{L}^{\mathrm{T}} & \mathbf{I} \end{bmatrix}_{(n+k) \times (n+k)} \tag{51}$$

$$\mathbf{\Gamma_i} = \mathrm{diag}\left(\gamma_{i,1}, \gamma_{i,2}, ...\gamma_{i,k}\right) \tag{52}$$

$$\mathbf{I}^{\mathrm{T}} = (1, 1, ..., 1)_{k \times k} \tag{53}$$

In the state-space representation, the displacements $\mathbf{x}$, $\mathbf{u}$ and the velocities $\dot{\mathbf{x}}$, $\dot{\mathbf{u}}$ of the system are composed in the state vector $\mathbf{z}$ and its first derivative $\dot{\mathbf{z}}$ as

$$\mathbf{z}^{\mathrm{T}} = (\mathbf{x}, \mathbf{u}, \dot{\mathbf{x}}, \dot{\mathbf{u}})_{2 \cdot (n+k) \times 1}, \tag{54}$$

$$\dot{\mathbf{z}}^{\mathrm{T}} = (\dot{\mathbf{x}}, \dot{\mathbf{u}}, \ddot{\mathbf{x}}, \ddot{\mathbf{u}})_{2 \cdot (n+k) \times 1}. \tag{55}$$

Using the state vector $\mathbf{z}$ and its first derivative $\dot{\mathbf{z}}$, a general representation of a horizontally excited MDoF system with several S-TLCDs is derived. The distribution vector $\mathbf{e_g}$ and the distribution matrix $\mathbf{E}$ are provided in Eq. 57 and 58:

$$\dot{\mathbf{z}} = \mathbf{A_r} \cdot \mathbf{z} - \mathbf{e_g}\, \ddot{x}_g + \mathbf{E} \cdot \mathbf{f}, \tag{56}$$

$$\mathbf{e_g} = \begin{bmatrix} \mathbf{0} \\ \mathbf{0} \\ \mathbf{M_M^{-1}} \begin{bmatrix} \mathbf{M_S} \cdot \mathbf{r} + \mathbf{L} \cdot \mathbf{M_D} \cdot \mathbf{i} \\ \mathbf{\Gamma_1} \cdot \mathbf{i} \end{bmatrix} \end{bmatrix}_{2 \cdot (n+k) \times n}, \tag{57}$$

$$\mathbf{E} = \begin{bmatrix} \mathbf{0} \\ \mathbf{0} \\ \mathbf{M_M^{-1}} \begin{bmatrix} \mathbf{I} \\ \mathbf{0} \end{bmatrix} \end{bmatrix}_{2\cdot(n+k)\times n} . \tag{58}$$

The hypermatrix $\mathbf{A_r}$ defines dynamic properties of the system and consists of two further components $\mathbf{A}$ and $\mathbf{B}\cdot\mathbf{R}$ as given below in Eq. 60-62:

$$\mathbf{A_r} = \mathbf{A} + \mathbf{B}\cdot\mathbf{R}, \tag{59}$$

$$\mathbf{A} = \begin{bmatrix} \mathbf{0} & \mathbf{I} \\ -\mathbf{M_M^{-1}} \cdot \begin{bmatrix} \mathbf{K_S} & \mathbf{0} \\ \mathbf{0} & \mathbf{0} \end{bmatrix} & -\mathbf{M_M^{-1}} \cdot \begin{bmatrix} \mathbf{C_S} & \mathbf{0} \\ \mathbf{0} & \mathbf{0} \end{bmatrix} \end{bmatrix}_{2\cdot(n+k)\times 2\cdot(n+k)} , \tag{60}$$

$$\mathbf{B} = \begin{bmatrix} \mathbf{0} & \mathbf{I} \\ -\mathbf{M_M^{-1}} \cdot \begin{bmatrix} \mathbf{I} & \mathbf{0} \\ \mathbf{0} & \mathbf{I} \end{bmatrix} & -\mathbf{M_M^{-1}} \cdot \begin{bmatrix} \mathbf{I} & \mathbf{0} \\ \mathbf{0} & \mathbf{I} \end{bmatrix} \end{bmatrix}_{2\cdot(n+k)\times 2\cdot(n+k)} , \tag{61}$$

$$\mathbf{R} = \begin{bmatrix} \mathbf{0} & \mathbf{0} & \mathbf{0} & \mathbf{0} \\ \mathbf{0} & \mathbf{K_D} & \mathbf{0} & \mathbf{0} \\ \mathbf{0} & \mathbf{0} & \mathbf{0} & \mathbf{0} \\ \mathbf{0} & \mathbf{0} & \mathbf{0} & \mathbf{C_D} \end{bmatrix}_{2\cdot(n+k)\times 2\cdot(n+k)} . \tag{62}$$

## 4. Experimental Investigations

To verify the natural frequency equation derived in Section 3 and to show the proof of concept of the S-TLCD, experimental investigations are conducted at the control engineering laboratory of RWTH Aachen University. The study focuses on the natural frequency adaptation capability, effects on the inherent damping and the vibration control performance of the S-TLCD considering frequency tuning effects and influences of the geometric factors.

### *4.1. Experimental Setup*

The experimental setup consists of a small-scale model of the S-TLCD with full adaptation capability and a model structure, on which the S-TLCD is attached and excited by an uniaxial shaking table.

The model of the S-TLCD, as shown in Figure 5, has the intended adaptation features and can change its natural frequency and damping behaviour. For the U-shaped tank, acrylic glass is chosen to allow visual observation of the liquid motion and position change of the movable components. The tank is built by rectangular glass elements, which are glued with each other, compressed by screws and sealed with silicone. The tank is 430 mm length, 570 mm height and 130 mm width. The material thickness of the acrylic glass is 15 mm. The cross-sectional area of the vertical columns of the tank is 50 mm × 100 mm. The horizontal passage has a cross-sectional area of 100 mm × 100 mm.

The S-TLCD model has in each vertical column two movable panels, which can change the cross-sectional area of the vertical columns and allow the tuning of the natural frequency, see ① in Figure 5 and Figure 6. Each panel consists of two segments, which are connected by joints. The first transition segment is 60 mm long and connects the second segment with the vertical column of the tank. The second segment is vertical and has a length of 385 mm. In each vertical column, the panels are connected together with a threaded rod, which allows the panels to change their position simultaneously perpendicular to the liquid flow and accordingly to the operation direction of the S-TLCD. Each threaded rod is connected to an actuator, which

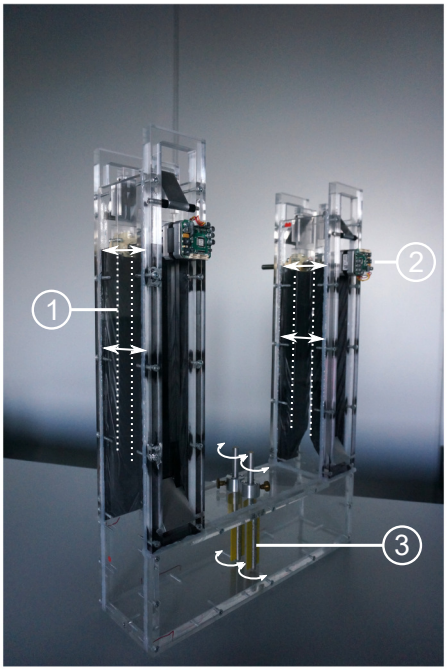


Figure 5: S-TLCD model. ①: Movable panels for natural frequency tuning. ②: Actuators adjusting the panels. ③: Butterfly valves for damping tuning.

allows an electronic adjustment of the panel positions, see ② in Figure 5 and Figure 6. The gaps between the panels and the tank walls are sealed with water-resistant and highly-expandable plastic membranes. The construction allows the panels to change their position within a range of $\beta = [45°, 72°]$.

For the tuning of the inherent damping, two butterfly valves are installed in the middle of the horizontal passage, see ③ in Figure 5 and ④ in Figure 6. Each valve consists of a rectangular plate with the dimensions 98 mm × 45 mm. Each plate is rotatable around a vertical axis perpendicular to the liquid flow direction. By opening the valves (rotation angle of the plate $\varphi = 90°$) and closing them ($\varphi = 0°$), the inherent damping can be changed due to modulation of the local friction effects. As shown in Figure 6 by ⑤, both valves are connected by gear wheels to an actuator, which allows a simultaneous electronic adjustment of the valves.

For the measurement of the liquid motion, a capacitance transducer is developed and installed in one of the vertical columns of the S-TLCD model, which can dynamically measure the liquid level change, see ③ in Figure 6. The liquid motion is recorded at a sample rate of 100 Hz allowing the identification of relevant dynamic parameters, such as maximum liquid amplitude and natural frequency of the S-TLCD. The measured liquid motion is also utilized to investigate the inherent damping effects of the S-TLCD.

For the experimental investigations, a uniaxial horizontal shaking table is built, which can generate harmonic vibrations, see ③ in Figure 7. The shaking table is operated by a linear actuator in a frequency range of 0.1 - 50 Hz with 100 mm (±50 mm) stroke. The motion of the shaking table is registered by a microelectromechanical system (MEMS) accelerometer. During the experimental investigations, the S-TLCD is directly attached on the shaking table to study its natural frequency and inherent damping. During further tests regarding the performance of the damper, the S-TLCD is attached to a model structure, which is excited by the shaking table as shown in Figure 7.

The model structure consists of a pendulum attached to a rigid frame with four steel wires, see ② in Figure 7. The rigid frame is built by aluminium elements and has its natural frequency at 9.20 Hz. The pendulum consists of a platform, where the S-TLCD can be attached and has its natural frequency at

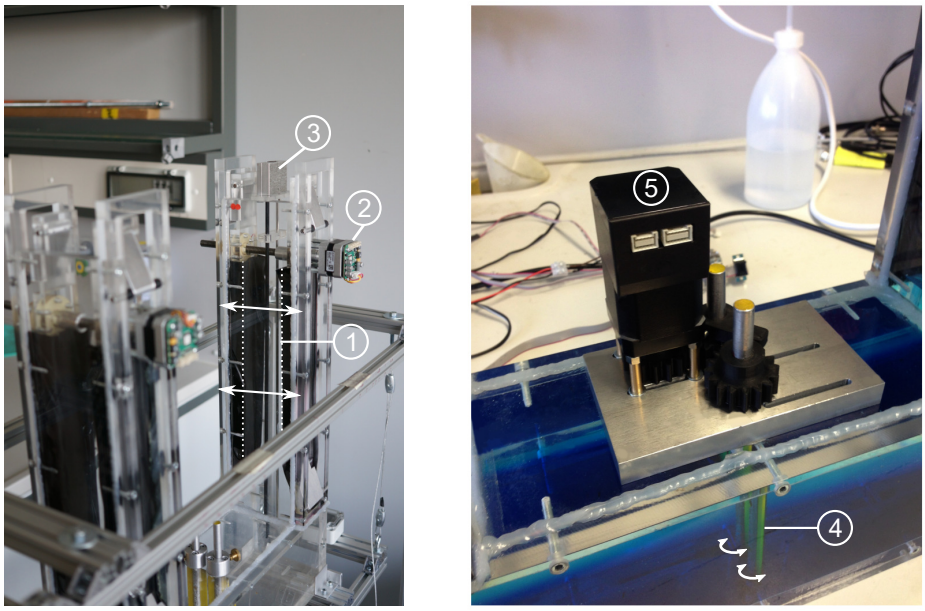


Figure 6: The actuator of the butterfly valves to control the inherent damping of S-TLCD. S-TLCD attached on the pendulum of the model structure (Left). S-TLCD filled with liquid (water and colorant) (Right) ①: Movable panels for frequency tuning. ②: Actuators adjusting the movable panels. ③: Sensor measuring the liquid motion. ④: Buttelfly valves for damping tuning. ⑤: Actuator adjusting the valves.

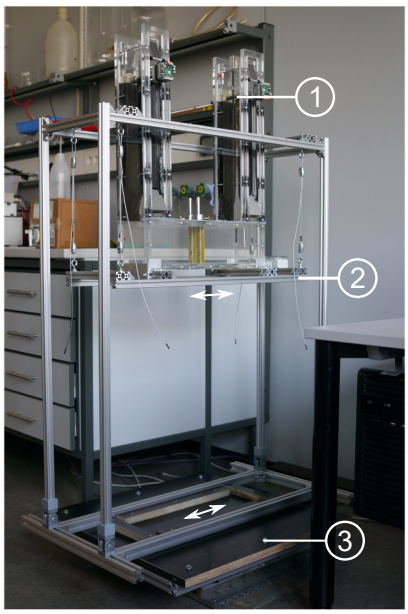


Figure 7: Model structure on shaking table with the S-TLCD. ①: S-TLCD model. ②: Pendulum connected to a rigid frame structure, which is excited by the shaking table in horizontal direction. ③: Uniaxial shaking table.

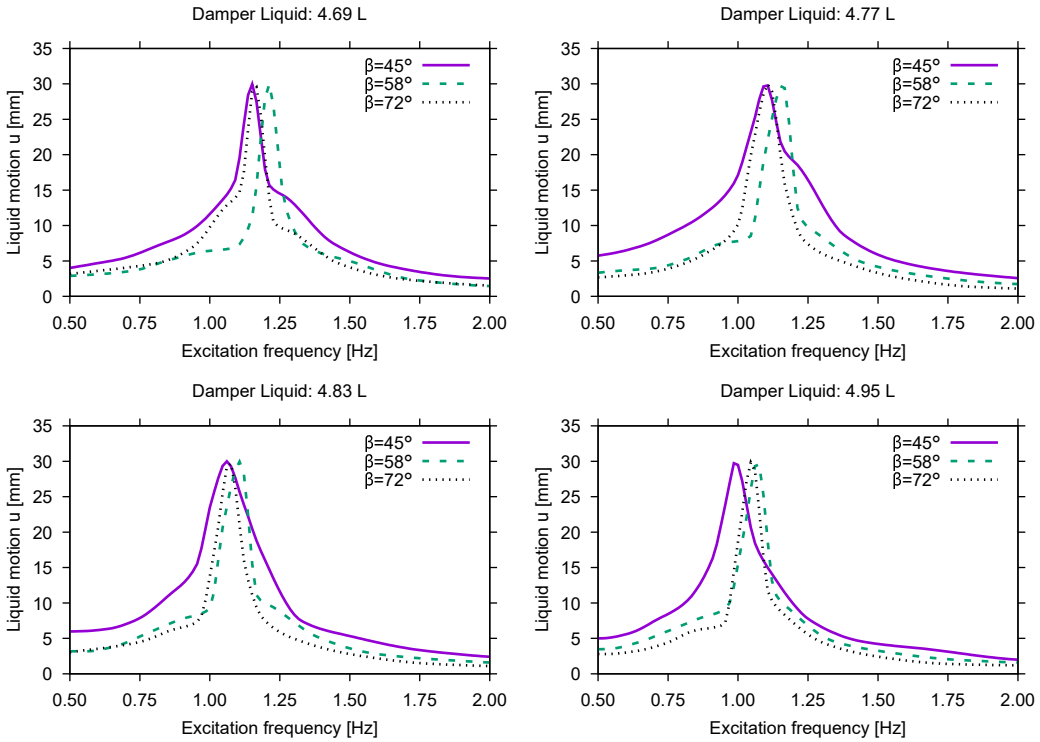


Figure 8: Frequency response spectra of the four damper configurations with the liquid volumes 4.69, 4.77, 4.83 and 4.95 L at the panel positions 45°, 58° and 72°. The butterfly valve position is $\varphi = 0°$ (closed).

$f_S = 1.15$ Hz, which can be changed by modifying the length of the wires. The damping ratio of the pendulum is about $D = 1.0\%$. The mass of the pendulum together with the mass of the S-TLCD are documented in Section 4.4.1 and Table 4. The motion of the pendulum is registered also by a MEMS accelerometer. The model structure with the pendulum simulates a horizontally oscillating SDoF system with a low natural frequency, which allows the design of a very compact S-TLCD utilizing reasonable actuators adequate for the laboratory environment, where the tests are conducted.

### *4.2. Investigations on the Natural Frequency*

For the verification of the natural frequency equation of the S-TLCD, four damper configurations with the liquid volumes 4.69, 4.77, 4.83 and 4.95 L. with variable panel positions are investigated. During these investigations, the S-TLCD model is directly attached on the shaking table and excited harmonically by excitation frequencies 0.50-2.00 Hz with an increment of 0.10 Hz. For each damper configuration the experiments are repeated for panel positions between 45° and 72° with an increment of 0.5°. The damper response is determined by measuring the liquid motion. From the maximum values of the liquid motion, the frequency response curves for the conducted frequency sweeps are determined. Figure 8 shows the measured frequency response curves for the tested four damper configurations and selected panel positions 45°, 58° and 72°. The peak values of the frequency curves correspond to the resonant response of the damper, in which the excitation frequency matches with the natural frequency. From the corresponding frequency the natural frequency of the damper is determined.

In Figure 8, the change of the natural frequency is clearly observed from the horizontal shift of the peak of the frequency response curve. The shape of the frequency response curve shows that the panel position has also a certain effect on the damping ratio of the damper. The wide frequency curve at the panel position 45° indicates more damping compared to the panel positions 58° and 72°. Further discussion regarding this damping effect can be found in Section 4.3.

Table 1: Parameters of the S-TLCD configuration with 4.69 and 4.95 L liquid volume and comparison of the calculated natural frequency $f_{D,c}$ with the measured natural frequency $f_{D,m}$.

| $\beta$ [°] | $V_1$ [m] | $V_2$ [m] | $V_3$ [m] | $H$ [m] | $A_{V1}$ [m$^2$] | $A_{V2}$ [m$^2$] | $A_H$ [m$^2$] | $L_1$ [m] | $f_{D,c}$ [Hz] | $f_{D,m}$ [Hz] |
|---|---|---|---|---|---|---|---|---|---|---|
| 4.69 L | | | | | | | | | | |
| 45 | 0.050 | 0.042 | 0.115 | 0.350 | $0.18 \cdot 10^{-2}$ | $0.50 \cdot 10^{-2}$ | $1.00 \cdot 10^{-2}$ | 0.383 | 1.14 | 1.15 |
| 58 | 0.050 | 0.051 | 0.052 | 0.350 | $0.28 \cdot 10^{-2}$ | $0.50 \cdot 10^{-2}$ | $1.00 \cdot 10^{-2}$ | 0.328 | 1.21 | 1.21 |
| 72 | 0.050 | 0.057 | 0.020 | 0.350 | $0.42 \cdot 10^{-2}$ | $0.50 \cdot 10^{-2}$ | $1.00 \cdot 10^{-2}$ | 0.373 | 1.15 | 1.16 |
| 4.95 L | | | | | | | | | | |
| 45 | 0.050 | 0.042 | 0.189 | 0.350 | $0.18 \cdot 10^{-2}$ | $0.50 \cdot 10^{-2}$ | $1.00 \cdot 10^{-2}$ | 0.531 | 0.97 | 0.99 |
| 58 | 0.050 | 0.051 | 0.098 | 0.350 | $0.28 \cdot 10^{-2}$ | $0.50 \cdot 10^{-2}$ | $1.00 \cdot 10^{-2}$ | 0.430 | 1.07 | 1.07 |
| 72 | 0.050 | 0.057 | 0.052 | 0.350 | $0.42 \cdot 10^{-2}$ | $0.50 \cdot 10^{-2}$ | $1.00 \cdot 10^{-2}$ | 0.436 | 1.07 | 1.06 |

For each damper configuration and panel position, the mathematical parameters are determined, as introduced in Section 3.1. From these parameters the natural frequencies are calculated by using equations of the natural frequency $\omega_D$ and first efficient length $L_1$, which are repeated below in Eq. 63 and Eq. 64. Table 1 shows the damper parameters for two damper configurations with 4.69 and 4.95 L, and compares the calculated and measured natural frequencies. In Figure 9, the calculated natural frequencies $f_{D,c}$ are compared with the measured natural frequencies $f_{D,m}$ for the tested four damper configurations within the operation range of the panels between 45° and 72°. The results correspond to each other very well proving the applicability of the mathematical equation of the natural frequency of S-TLCD.

$$f_{D,c} = \frac{1}{2\,\pi}\,\sqrt{\frac{2\,g}{L_1}} \tag{63}$$

$$L_1 = 2\,V_3 + V_2 + (2\,V_1 + V_2)\,\frac{A_{V1}}{A_{V2}} + H\,\frac{A_{V1}}{A_H} \tag{64}$$

### *4.3. Investigations on the Inherent Damping*

#### *4.3.1. Effects of the Butterfly Valves on the Inherent Damping*

For the investigation of the effects of the butterfly valves on the inherent damping of the S-TLCD four different valve positions are tested: $\varphi = \{0°, 30°, 60°, 90°\}$, where $\varphi = 0°$ corresponds to closed position and 90° to open. Each test is repeated for four times to increase the statistical accuracy of the results. The tests are performed on the S-TLCD configuration with 4.69 L at a panel position of $\beta = 45°$. The S-TLCD is attached directly on the shaking table and a free vibration of the liquid is induced by a sudden start and stop of the table after a certain initial velocity. For this purpose, the motion of the shaking table is tuned in such a way that the first peak of the liquid motion is approximately $u_{max} \approx 15$ mm. As shown in Figure 10, the damping ratios are determined from the recorded decay curves of the liquid motion beginning with this peak.

In Figure 10, the left diagram shows the comparison of the time histories for the open and closed valve positions. The measured initial liquid motion peaks of the shown data sets are $u = 14.97$ mm for the valve in closed position and $u = 15.24$ mm for the valve in open position. The decay of the liquid deflection increases by closing the valve, which shows the increased damping behaviour. The right diagram shows the determined damping ratios, which vary between 4.6% and 7.4% for the tested valve positions. The test results prove that the damping ratio of the S-TLCD can be modified efficiently by changing the valve position.

For the investigation of the effects coming from the nonlinearity of the S-TLCD damping and its coherence with the deflection amplitude, further tests are conducted with higher liquid deflection amplitudes. For this

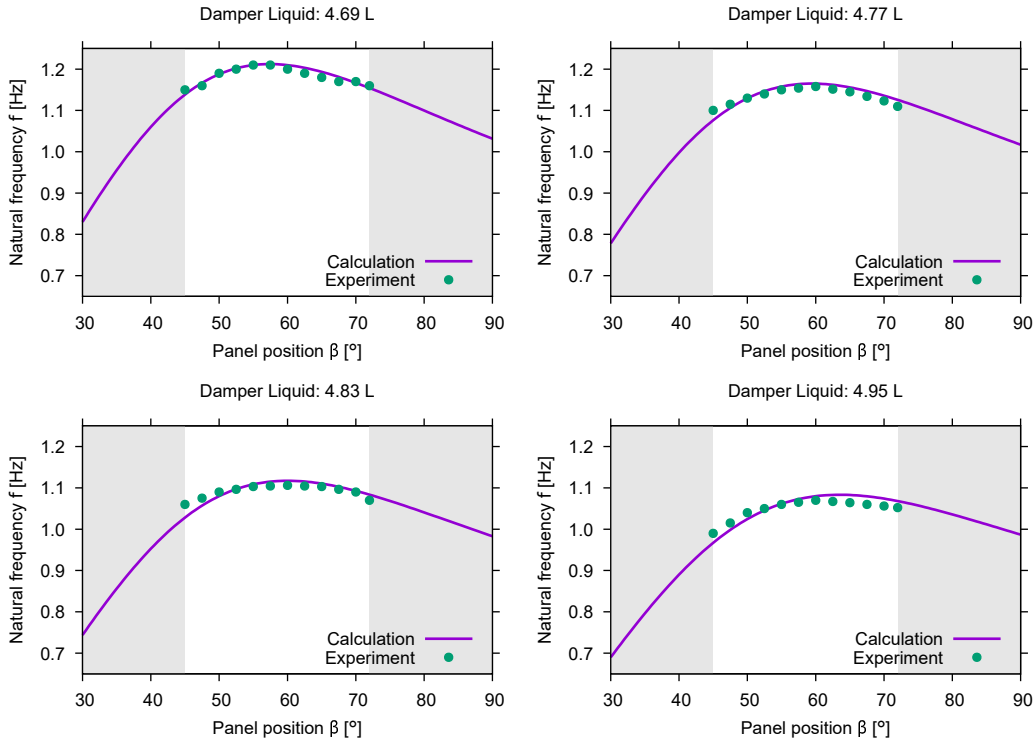


Figure 9: Comparison of analytical and experimental results showing the relationship between the natural frequency and the panel position for four damper configurations with liquid volumes: 4.69, 4.77, 4.83 and 4.95 L. The non-grey areas are showing the operation range of the panels. The butterfly valve position is $\varphi = 0°$ (closed).

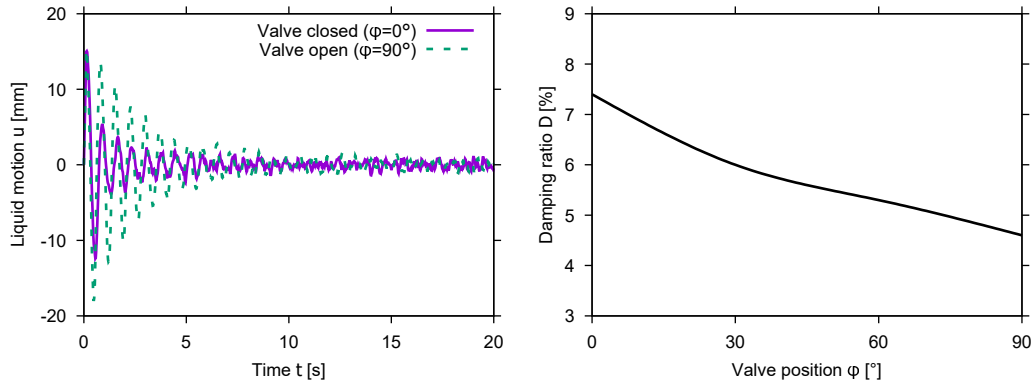


Figure 10: Time histories of the liquid motion for the valve positions $\varphi = 0°$ and $\varphi = 90°$ (Left). Relationship between the damping ratio $D$ and the valve position $\varphi$ determined from time series with $u_{max} \approx 15$ mm and 5 oscillations (Right). The panel position is $\beta = 45°$.

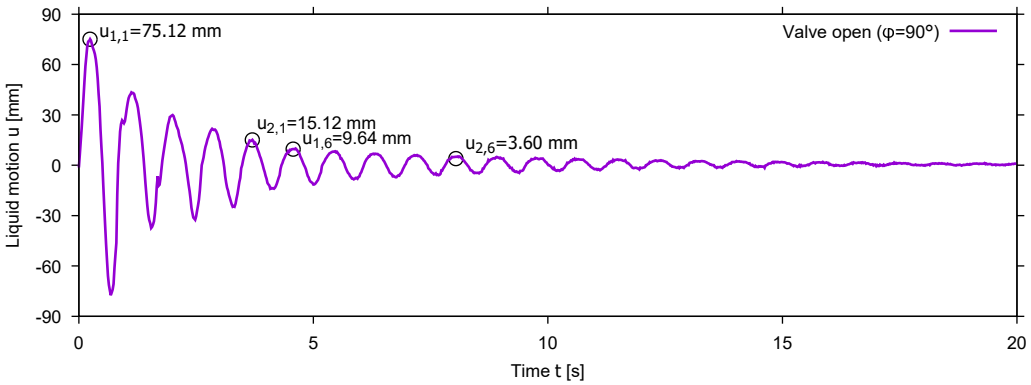


Figure 11: Investigation of the nonlinearity depending on the damping ratio and the liquid motion amplitude. The panel position is $\beta = 45°$.

Table 2: Parameters of the experimental investigations on the nonlinear inherent damping effects of the S-TLCD.

| | $u_i$ [mm] | $u_{i+n}$ [mm] | $n$ [-] | $\Lambda$ [-] | $D$ [%] |
|---|---|---|---|---|---|
| Data set 1 | 75.12 | 9.64 | 5 | 0.41 | 6.5 |
| Data set 2 | 15.12 | 3.60 | 5 | 0.29 | 4.6 |

purpose, the motion of the shaking table is increased, which caused an initial liquid motion peak of $u = 75.12$ mm, as shown in Figure 11. During these tests, the valve position is set as $\varphi = 90°$ (open). The damping ratios are determined from several decay curves using different amplitude combinations. For the amplitude pairs 75.12-9.64 mm and 15.12-3.60 mm the determined damping ratios are 6.5% and 4.6% as evaluated in Table 2, where $u_i$ and $u_{i+n}$ are the amplitude pairs, $n$ is the number of oscillations between the amplitude pairs, $\Lambda$ is the logarithmic decrement and $D$ is the damping ratio of the S-TLCD. It is evident from these results, that for larger amplitudes the damping ratio increases slightly in a nonlinear manner.

Due to the nonlinearity of the inherent damping, for real applications, the tuning of the damping requires a mapping of the relationship between the liquid stream velocity amplitude and the damping term $\delta|\dot{u}|\dot{u}$. Sophisticated control algorithms, such as using soft-computing methods can conduct this [32]. This approach can consider the nonlinearity of the damper and allow an accurate tuning of the damping depending on the liquid velocity. On the other hand, es explained in Section 3, the nonlinear damping term of the equation of motion can also be linearized by introducing the equivalent damping ratio $D_D$. This approximation approach, which was proposed in [31], has sufficient accuracy at least for harmonic excitations with low liquid amplitudes. At higher amplitudes or random excitations, the linearization underestimates the inherent damping and cause mistuning effects, which will sink the performance of the damper.

*4.3.2. Effects of the Movable Panels on the Inherent Damping*

For the investigation of the effects of the movable panels on the inherent damping of the S-TLCD further tests were conducted for the three different panel positions at 45°, 58° and 72° using the damper configuration with 4.69 L and a constant valve position at 90° (open). Further parameters are shown in Table 3. Similar to the previous investigations on the valve effects, the damping ratios are determined from the deflection decay curves of the liquid motion. Figure 12 (Left) shows the time histories of the liquid deflection for the tested three panel positions and the amplitude pairs, which are used for the determination of the damping ratios. The highest damping ratio with 6.5% was determined for 45°. The lowest damping ratio is 4.8% at panel position 72°. By closing the panels the damping ratio increases. This result matches with the previous results from frequency sweep tests, which are presented in Section 4.2. During frequency sweeps, the measured frequency response curve of the panel position 45° was wider than of the panel positions 58°

Table 3: Parameters of the experimental investigations on the damping effects caused by the panels.

| $\beta$ [°] | $u_i$ [mm] | $u_{i+n}$ [mm] | $n$ [-] | $\Lambda$ [-] | $D$ [%] |
|---|---|---|---|---|---|
| 45 | 75.12 | 9.64 | 5 | 0.41 | 6.5 |
| 58 | 75.10 | 14.98 | 5 | 0.32 | 5.1 |
| 72 | 75.14 | 16.44 | 5 | 0.30 | 4.8 |

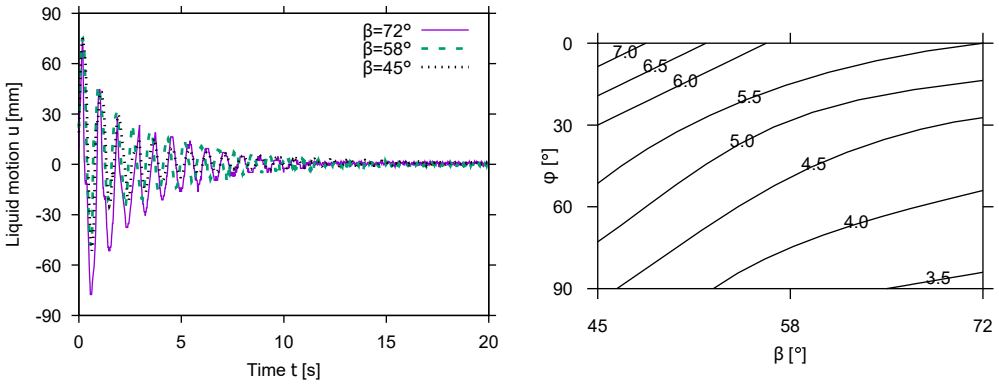


Figure 12: Investigation of the effect of the panel position on the damping behaviour. Valve position is $\varphi = 90°$ (open) (Left). Damping ratio [%] of the S-TLCD for different valve/panel ($\varphi/\beta$) positions determined from time series with $u_{max} \approx 15$ mm using 5 oscillations (Right).

and 72° showing that the damping behaviour is affected not only by the valves but also by the panel position, cf. Figure 8.

As mentioned previously in Section 2, the inherent damping of the S-TLCD is caused by local friction effects in the tank. Therefore, every tank component, which is introducing additional friction, leads to a complementary increase in the inherent damping.

To investigate this effect, we firstly changed in Section 4.3.1 only the position of the butterfly valves. As shown in Section 4.3.1, at the panel position $\beta = 45°$, the inherent damping decreases by just opening the butterfly valves from $\varphi = 0°$ to 90°. This effect is known also from the conventional TLCDs.

Secondly, we changed in Section 4.3.2 also the panel position. As shown in this section, the inherent damping decreases further also by opening the movable panels from $\beta = 45°$ to 72°. This effect is unique for the S-TLCD.

To investigate the interaction between the valve and panel positions $\varphi$ and $\beta$ in more detail, we conducted further tests. During these tests, we determined the damping ratio for different $\varphi$ and $\beta$ from decay curves with $u_{max} \approx 15$ mm using 5 oscillations. The results are shown in Figure 12 (Right). As determined also previously, the S-TLCD reaches the maximum damping ratio at a valve position of $\varphi = 0°$ (closed) with a panel position of $\beta = 45°$. By opening the valves to $\varphi = 90°$ and the panels to $\beta = 72°$ the S-TLCD reaches its minimum damping ratio. The determined maximum and minimum damping ratios are 7.4% and 3.4% respectively. Other variations, as also shown in Figure 12, lead to damping ratios, which are between these two limit values. It is worth noting that the inherent damping of the S-TLCD, as previously discussed in Section 4.3.1 and shown in Figure 11, also depends on the amplitude of the liquid motion.

### *4.4. Investigations on the Vibration Control Performance*

The following sections will present the results of the investigations on the vibration control performance of the S-TLCD. As mentioned in Section 1, the damping adaptation using an orifice, as proposed by [8], counts as an established method, which is also utilized in the S-TLCD in a similar manner by the butterfly valves. Studies on the performance effects of this approach can be found in the literature such as in [10, 11].

Table 4: Parameters of the performance study.

| $\beta$ [°] | $f_D(\beta)$ [Hz] | $f_S$ [Hz] | $m_D$ [kg] | $m_{Pe}$ [kg] | $m_{De}$ [kg] | $m_S = m_{Pe} + m_{De}$ [kg] |
|---|---|---|---|---|---|---|
| $45 - 72$ | $0.97 - 1.07$ | 1.15 | 4.950 | 1.500 | 9.360 | 10.860 |

The major novelty of the proposed S-TLCD is its frequency adaptation capability. Therefore, and for the sake of brevity, this paper focuses on the effects of the frequency adaptation on the performance of the S-TLCD. In this regard, Section 4.4.1 discusses the effects of the natural frequency tuning on the damper performance. Section 4.4.2 documents the side effects of the frequency adaptation, which are initiated by the change of geometric factors.

*4.4.1. Effects of the Natural Frequency Tuning on the Damper Performance*

The natural frequency tuning is decisive for the efficiency of structural control systems utilizing auxiliary masses. As a semi-active system, the S-TLCD is able to change its natural frequency and is therefore expected to reach a higher performance compared to a passive detuned damper. This effect is investigated during an experimental campaign with the S-TLCD.

During these tests, the S-TLCD with 4.95 L liquid amount is attached on the pendulum. As experimentally determined in Section 4.2, this S-TLCD configuration can change its natural frequency within the range of 0.97 Hz to 1.07 Hz. For a 1.15 Hz pendulum natural frequency the optimum natural frequency is determined using the system parameters documented in Table 4 according to the Den Hartog criteria [35] given in Eq. 65 - 68 for the S-TLCD. In Table 4, $f_D$ is the natural frequency of the damper depending on the panel position $\beta$ and $f_S$ is the natural frequency of the pendulum. Further parameters introduced in Table 4 are the liquid mass of the damper $m_D$, the mass of the pendulum $m_{Pe}$ and the mass of the damper prototype $m_{De}$. As $m_{Pe}$ and $m_{De}$ are "dead masses", the vibration of which is aimed to be controlled, these masses are compiled in $m_S$ and called as the main mass, whereas $m_D$ is the secondary mass.

As derived in Section 3.3 and shown in Eq. 65, the amount of liquid mass, which is actively participating to the vibration control, is calculated by scaling the total liquid mass $m_D$ with the geometric factors $\gamma_1$ und $\gamma_2$. The rest liquid mass is also a "dead mass", which is necessary only for the tuning of the natural frequency of the damper. Therefore, this mass is added in Eq. 66 to the main mass $m_S$. In Eq. 66, the mass ratio $\bar{\mu}$, which is necessary for the application of the Den Hartog criteria, is calculated from the actively participating liquid mass $\bar{m}_D$ and the total amount of the dead mass $\bar{m}_S$. This mass ratio together with the natural frequency of the system $f_S$ is substituted in Eq. 68 to determine the optimum natural frequency of the damper. The pendulum, on which the S-TLCD model is attached, can be assumed to be a mathematical pendulum, the natural frequency of which is independent from the mass. Therefore, in Eq. 68, the natural frequency $f_S$ is not changed by the additional mass.

$$\bar{m}_D = m_D \, \gamma_1 \, \gamma_2 \tag{65}$$

$$\bar{\mu} = \frac{\bar{m}_D}{\bar{m}_S} = \frac{m_D \, \gamma_1 \, \gamma_2}{m_S + m_D \, (1 - \gamma_1 \, \gamma_2)} = \frac{\mu \, \gamma_1 \, \gamma_2}{1 + \mu \, (1 - \gamma_1 \, \gamma_2)} \tag{66}$$

$$\mu = \frac{m_D}{m_S} \tag{67}$$

$$f_{D,opt} = \frac{f_S}{1 + \bar{\mu}} \tag{68}$$

The optimum inherent damping of the S-TLCD can be approximated in a similar manner to the frequency tuning according to the Den Hartog criteria. The result will be a linearized damping ratio as given in Eq. 69, where $\bar{\mu}$ is again the mass ratio of actively participating liquid mass $\bar{m}_D$ and the total amount of the

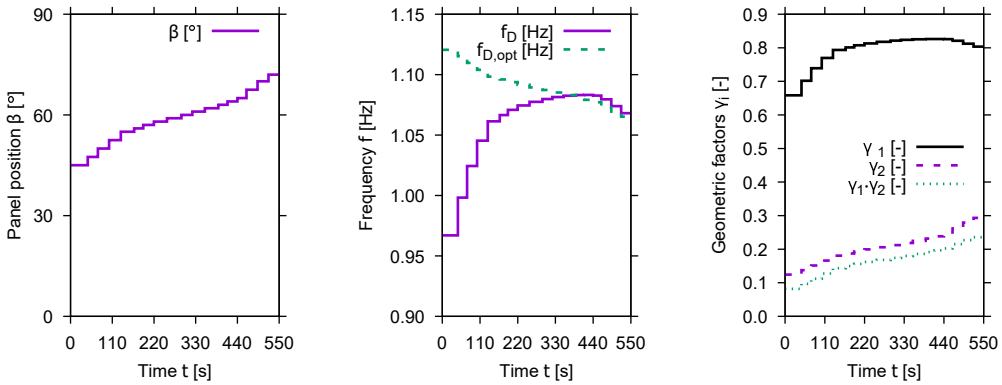


Figure 13: Time history of the panel position $\beta$ (Left) influencing the natural frequency $f_D$ and the geometric factors $\gamma_i$. Change of $f_D$ compared with the optimum natural frequency $f_{D,opt}$ (Centre). Change of $\gamma_1$ and $\gamma_2$ (Right).

dead mass $\bar{m}_M$.

$$D_{D,opt} = \sqrt{\frac{3\bar{\mu}}{8(1+\bar{\mu})^3}} \tag{69}$$

As stated before, $\bar{\mu}$ depends on the geometric factors $\gamma_1$ and $\gamma_2$. As shown in Figure 13, a position change of the movable panels initiates a change of the geometric factors, which will be discussed in Section 4.4.2 in detail. This change in the geometric factors has according to Eq. 69 also an influence on the optimum damping ratio. In this study, the influence of geometric factors on the optimum damping ratio is neglected and the damping ratio kept constant by adjusting the butterfly valves to the closed position with $\varphi = 0°$.

For the investigation of the frequency tuning effect, the pendulum and S-TLCD system is excited harmonically by the shaking table with the natural frequency of the pendulum inducing resonant vibrations. During the excitation, the panel position $\beta$ is changed gradually in its operation range of 45°-72°. Figure 13 (left) shows the time history of $\beta$ for a test sequence of 550 seconds. Figure 13 (centre) shows for the same test sequence the time history of the measured natural frequency $f_D$ and the calculated optimum natural frequency $f_{D,opt}$ of the damper according to Den Hartog. As illustrated in this diagram, $f_D$ catches $f_{D,opt}$ exactly with 1.083 Hz at $\beta = 62°$. At $\beta = 72°$, $f_D$ comes also very close to $f_{D,opt}$ by 1.068 Hz compared to 1.065 Hz. Figure 13 (right) shows for the same test sequence the time history of the calculated geometric factors $\gamma_1$, $\gamma_2$ and their multiplication $\gamma_1 \cdot \gamma_2$. As discussed in Section 3.3, with changing panel position the natural frequency and the geometric factors change in a nonlinear manner.

Figure 14 (left) shows the time history of the measured acceleration of the pendulum. The maximum acceleration is observed at the beginning of the test sequence due to the detuned natural frequency of the damper. At $\beta = 45°$, the natural frequency of the damper is 0.97 Hz and the optimum frequency is 1.12 Hz. As the natural frequency comes closer to the optimum frequency, the acceleration reduces. However, the minimum acceleration 0.032 $m/s^2$ is reached at the panel position $\beta = 72°$, rather than at $\beta = 62°$, where the natural frequency is exactly equal the optimum frequency. At $\beta = 62°$, the acceleration is measured as 0.037 $m/s^2$. This effect is caused by the geometric parameters $\gamma_1$ and $\gamma_2$ due to increased amount of active mass fraction $\bar{m}_D$, which will be discussed in the next Section 4.4.2.

A sample of the liquid motion time history, which is measured during the investigations, is shown in Figure 14 (right). The liquid oscillation decreases as the pendulum vibration decreases. Also this effect will be discussed in the next Section 4.4.2.

The effects of the frequency tuning is determined by comparing the measured maximum and minimum pendulum accelerations shown in Figure 14 (left). As a result, during the experimental investigations, the frequency adaptation capability of S-TLCD enabled a performance improvement of over 77%.

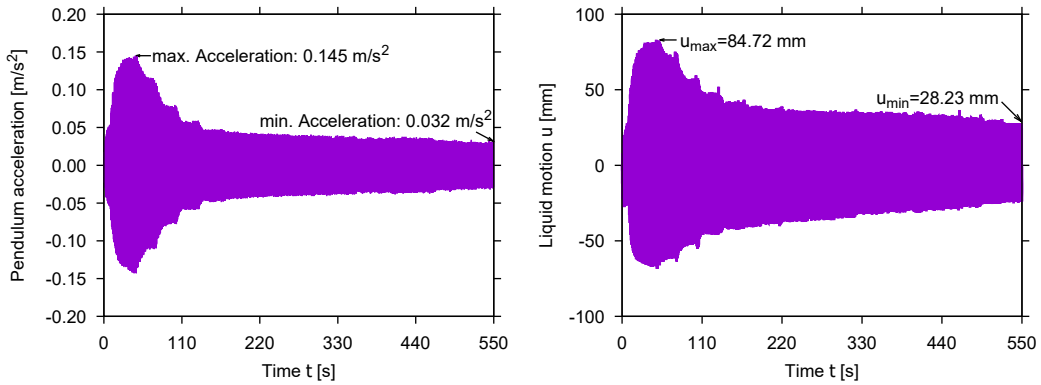


Figure 14: Time history of the pendulum acceleration induced by resonant harmonic excitation (Left). Time history of the liquid motion of the damper (Right).

*4.4.2. Effects of the Geometric Factors on the Damper Performance*

As derived in Section 3, the geometric factors, $\gamma_1$ and $\gamma_2$, determine the amount of active liquid mass $\bar{m}_D$ participating to the vibration control. Therefore, besides frequency tuning effects, they are both expected to have an influence on the performance of the damper. Furthermore, $\gamma_1$ is directly connected with the effective length $L_1$, which determines the natural frequency $\omega_D$. Therefore, it is expected to have a close correlation with the damper performance. $\gamma_2$ scales the restoring force, as shown in Eq. 39. Therefore, it is also expected to be relevant for the performance of the damper. As mentioned in Section 4.4.1, in this study the damping ratio is tuned by the butterfly valves with $\varphi = 0°$.

Figure 15 (left) shows the change of the geometric factors depending on the panel position $\beta$. The diagram in Figure 15 (centre) shows the frequency detuning determined from the frequency difference $\Delta f$ between the optimum damper frequency $f_{D,opt}$ and the natural frequency of the damper $f_D$. In Figure 15 (right) the S-TLCD induced reduction of the pendulum acceleration is illustrated. From the shape of the three curves, $\gamma_1$, $\Delta f$ and $R$, the direct correlation between these parameters can be observed. Compared to these three curves, the two other curves, $\gamma_2$ and $\gamma_1 \cdot \gamma_2$, are showing a different progress as the panel position changes.

To investigate this effect, the relevant parameters are compiled in Table 5 for discrete panel positions $\beta$. The shown parameters are the natural frequency of the damper $f_D$ and the optimum frequency $f_{D,opt}$, the maximum liquid deflection $u_{max}$ and the maximum pendulum acceleration $\ddot{x}_{max}$.

From these parameters the correlation coefficients are calculated to investigate the relationship between the parameters. The correlation coefficient of the frequency detuning $\Delta f = f_{D,opt} - f_D$ with the acceleration reduction $R$ is $-0.992$, which shows an almost full correlation. The correlation between the first geometric factor $\gamma_1$ and $R$ is about 0.971. The correlation between $\gamma_2$ and $R$ is 0.893. Comparing these three correlation values, it can be seen, that the frequency detuning has the highest effect on the damper performance. The standard deviations of the compared data sets of $\Delta f$, $\gamma_1$ and $\gamma_2$ are 0.052, 0.056 and 0.059 respectively, which are almost equal showing a comparable data distribution for the investigated parameters. These results match with the mathematical background derived in Section 3 and with the interpretations at the beginning of this section.

## 5. Conclusions

A new-type semi-active tuned liquid column damper (S-TLCD) is proposed to mitigate the lateral vibrations of high-rise civil engineering structures. The S-TLCD comprises a U-shape tank, which is partially filled with a Newtonian fluid. The S-TLCD provides mechanisms for the real-time continuous tuning of both natural frequency and damping parameters.

In the first part of the paper the governing equations of the S-TLCD are derived based on the non-stationary incompressible liquid flow. The equation of motion is compiled first for a SDOF system with

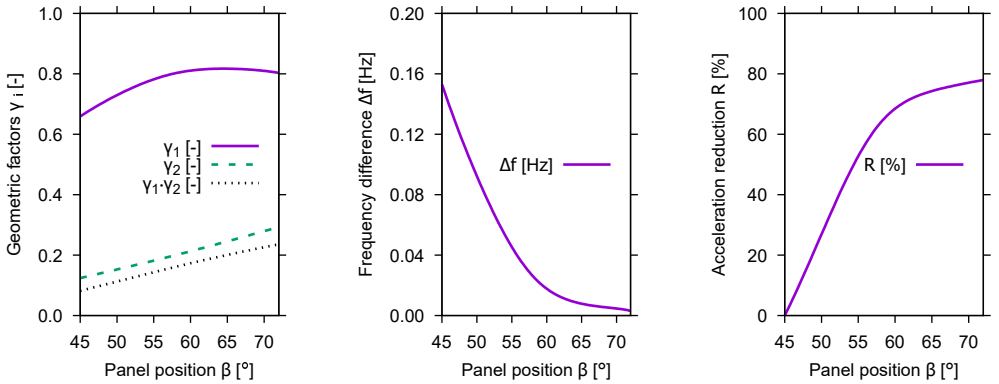


Figure 15: Change of the geometric parameters $\gamma_1$ and $\gamma_2$ depending on the panel position $\beta$ (left). Frequency detuning $\Delta f = f_{D,opt} - f_D$ in relevance to the panel position $\beta$ (centre). Comparison of the panel position $\beta$ induced natural frequency tuning effect and reduction of pendulum acceleration (right).

Table 5: Change of damper performance depending on frequency tuning $f_{D,opt} - f_D$ and geometric factors $\gamma_i$.

| $\beta$ [°] | $f_D$ [Hz] | $f_{D,opt}$ [Hz] | $u_{max}$ [mm] | $\ddot{x}_{max}$ $[m/s^2]$ |
|---|---|---|---|---|
| 45 | 1.12 | 0.97 | 143 | 0.145 |
| 50 | 1.11 | 1.02 | 75 | 0.110 |
| 55 | 1.10 | 1.06 | 57 | 0.059 |
| 60 | 1.09 | 1.08 | 36 | 0.040 |
| 65 | 1.08 | 1.08 | 34 | 0.037 |
| 70 | 1.07 | 1.07 | 33 | 0.033 |
| 72 | 1.07 | 1.07 | 30 | 0.032 |

a single S-TLCD. The natural frequency is formulated using a scaled liquid length. The scaling factors are derived from the tank geometry. Further geometric parameters, which influence the efficiency of the S-TLCD, are formulated. The interaction force between S-TLCD and structure is derived from the equation of momentum, which is induced by the liquid motion. For multi-degree-of-freedom (MDoF) systems with several S-TLCDs, the state-space representation is formulated allowing the simulation of S-TLCDs with MDoF systems including sensors and control algorithm.

In the second part of the paper the natural frequency equation is verified by experimental studies using a small-scale S-TLCD model attached to a shaking table. Further experiments are conducted to show proof of concept. The results show that the natural frequency of the S-TLCD can be controlled in the intended manner. Effects on the inherent damping of the S-TLCD are investigated. The results show that the inherent damping of the S-TLCD can also be controlled in the foreseen manner. Further experimental investigations are performed to study the effects influencing the control performance of the S-TLCD. For this investigation, the S-TLCD is attached to a model structure, which is excited by the shaking table. The results show that the tank geometry influences directly the efficiency of the damper. Hereby the most relevant aspect is revealed as the natural frequency tuning. During the experimental tests, the natural frequency adaptation capability enabled the S-TLCD a performance improvement of over 77%.

## 6. Future Work

The presented S-TLCD enables new possibilities for the application of new control algorithms, which can adapt both frequency and damping parameters. Furthermore, due to natural frequency adaptation capability, system identification algorithms are necessary, which can determine the relevant structural and loading parameter in real-time. Moreover, an optimum design of the S-TLCD requires multi-objective optimization algorithms, which can calculate the physical geometry parameters of the S-TLCD and its mechanisms.


## Acknowledgements

This research work is funded by the Excellence Initiative of the German federal and state governments. The authors would like to express their sincere appreciation for the support (Grant number: OPSF226). The authors would like to thank Control Engineering Institute of RWTH Aachen University for their support during the preparation of the experimental investigations. The authors also wish to thank Margarita Chasapi for her kind comments.


## References


[1] T. Kobori, M. Takahashi, T. Nasu, N. Niwa, K. Ogasawara, Seismic response controlled structure with active variable stiffness system, Earthquake Engineering and Structural Dynamics 22 (11) (1993) 925–941. doi:10.1002/eqe.4290221102.

[2] S. Nagarajaiah, Structural vibration damper with continuously variable stiffness (US Patent No. 6098969A, 2000).

[3] S. Nagarajaiah, Adaptive passive, semiactive, smart tuned mass dampers: Identification and control using empirical mode decomposition, hilbert transform, and short-term fourier transform, Structural Control and Health Monitoring 16 (7-8) (2009) 800–841. doi:10.1002/stc.349.

[4] C. Sun, S. Nagarajaiah, Study on semi-active tuned mass damper with variable damping and stiffness under seismic excitations, Structural Control and Health Monitoring 21 (6) (2014) 890–906. doi:10.1002/stc.1620.

[5] C. Sun, Semi-active control of monopile offshore wind turbines under multi-hazards, Mechanical Systems and Signal Processing 99 (2018) 285–305.

[6] C. Sun, Mitigation of offshore wind turbine responses under wind and wave loading: Considering soil effects and damage, Structural Control and Health Monitoring 25 (3) (2018) e2117.

[7] H. Frahm, Means for damping the rolling motion of ships (US Patent No. 970368, 1909).

[8] F. Sakai, S. Takaeda, T. Tamaki, Damping device for tower-like structure (US Patent No. 5070663, 1991).

[9] M. Matsuo, U-shaped tank type dynamic vibration absorbing device (JP Patent No. 09151986, 1986).

[10] S. K. Yalla, A. Kareem, Semiactive tuned liquid column dampers: Experimental study, Journal of Structural Engineering 129 (7) (2003) 960–971. doi:10.1061/(asce)0733-9445(2003)129:7(960).

[11] V. D. La, C. Adam, General on-off damping controller for semi-active tuned liquid column damper, Journal of Vibration and Control 5 (2016).

[12] D. D. A. Csupor, Passive stabilization tanks (US Patent No. 3678877, 1972).
[13] T. Nomichi, H. Yoshida, Vibration-proof structure in long span construction (JP Patent No. 01239205, 1989).
[14] M. Yoshimura, K. Yamazaki, Vibration damping device for vertical vibration (JP Patent No. 10220522, 1998).
[15] K. Kagawa, K. Fujita, Vibration isolation tank (JP Patent No. 02278033, 1990).
[16] K. Kagawa, H. Koukawa, K. Fujita, Y. Zensho, M. Matsuo, Development of tuned liquid damper for ship vibration, Transactions of the West-Japan Society of Naval Architects 78 (1989) 251–258.
[17] M. J. Hochrainer, F. Ziegler, Control of tall building vibrations by sealed tuned liquid column dampers, Structural Control and Health Monitoring 13 (6) (2006) 980–1002. doi:10.1002/stc.90.
[18] S. A. Mousavi, K. Bargi, S. M. Zahrai, Optimum parameters of tuned liquid column-gas damper for mitigation of seismic-induced vibrations of offshore jacket platforms, Structural Control and Health Monitoring 20 (3) (2013) 422–444. doi:10.1002/stc.505.
[19] C. Fu, Application of torsional tuned liquid column gas damper for plan-asymmetric buildings, Structural Control and Health Monitoring 18 (5) (2011) 492–509. doi:10.1002/stc.380.
[20] M. Reiterer, A. Kluibenschedl, Liquid damper for reducing vertical and/or horizontal vibrations in a building or machine structure (US Patent No. 20100200348A1, 2010).
[21] M. Reiterer, O. Altay, R. Wendner, S. Hoffmann, A. Strauss, Adaptive tuned liquid column dampers for structures, part ii: Field tests (in german), Stahlbau 77 (3) (2008) 205–212. doi:10.1002/stab.200810022.
[22] M. Yoshimura, K. Fujita, A. Teramura, Hydrostatic anti-vibration system and adjusting method therefor (US Patent No. 5542220A, 1996).
[23] K. Ahsan, K. Tracy, T. Yukio, Mitigation of motions of tall buildings with specific examples of recent applications, Wind and Structures 2 (3) (1999) 201–251. doi:10.12989/was.1999.2.3.201.
[24] A. Ghosh, B. Basu, Seismic vibration control of short period structures using the liquid column damper, Engineering Structures 26 (13) (2004) 1905–1913. doi:10.1016/j.engstruct.2004.07.001.
[25] H. Kim, H. Adeli, Hybrid control of smart structures using a novel wavelet-based algorithm, Computer-Aided Civil and Infrastructure Engineering 20 (1) (2005) 7–22. doi:10.1111/j.1467-8667.2005.00373.x.
[26] E. Sonmez, S. Nagarajaiah, C. Sun, B. Basu, A study on semi-active tuned liquid column dampers (stlcds) for structural response reduction under random excitations, Journal of Sound and Vibration 362 (2016) 1–15.
[27] K. W. Min, C. S. Park, J. Kim, Easy-to-tune reconfigurable liquid column vibration absorbers with multiple cells, Smart Materials and Structures 24 (6) (2015) 065041. doi:10.1088/0964-1726/24/6/065041.
[28] F. Ziegler, Mechanics of Solids and Fluids, Springer New York, 1995. doi:10.1007/978-1-4612-0805-1.
[29] F. Sakai, S. Takaeda, T. Tamaki, Tuned liquid column damper - new type device for suppression of building vibrations, Proc. of the Int. Conf. on High-rise Buildings, Nanjing 1 (1989) 926–931.
[30] S. D. Xue, J. M. Ko, Y. L. Xu, Tuned liquid column damper for suppressing pitching motion of structures, Engineering Structures 22 (11) (2000) 1538–1551. doi:Doi10.1016/S0141-0296(99)00099-1.
[31] M. Reiterer, F. Ziegler, Control of pedestrian-induced vibrations of long-span bridges, Structural Control and Health Monitoring 13 (6) (2006) 1003–1027. doi:10.1002/stc.91.
[32] N. Siddique, H. Adeli, Computational Intelligence: Synergies of Fuzzy Logic, Neural Networks and Evolutionary Computing, John Wiley and Sons, Inc., 2013.
[33] P. A. Hitchcock, K. C. S. Kwok, R. D. Watkins, B. Samali, Characteristics of liquid column vibration absorbers (lcva) i, Engineering Structures 19 (2) (1997) 126–134.
[34] P. A. Hitchcock, K. C. S. Kwok, R. D. Watkins, B. Samali, Characteristics of liquid column vibration absorbers (lcva) ii, Engineering Structures 19 (2) (1997) 135–144.
[35] J. P. D. Hartog, Mechanical Vibrations, McGraw-Hill Book Company, Inc., 1956.